Experimental Validation of Control Designs for Low-Loss Active Magnetic Bearings

Brian C. Wilson *

Air Force Research Laboratory, Kirtland AFB, NM, 87117-5776, USA

Panagiotis Tsiotras †

Georgia Institute of Technology, Atlanta, GA 30332-0150, USA

Bonnie Heck-Ferri ‡

Georgia Institute of Technology, Atlanta, GA 30332-0250, USA

This paper offers experimental validation of several recently developed nonlinear control laws, derived from the theory of integrator backstepping, control Lyapunov functions (CLF), and dissipativity, by implementing them on a spacecraft reaction wheel that is suspended by a low-loss active magnetic bearing (AMB). The electromagnets of the AMB are constrained by a generalized complementary flux constraint (GCFC). This constraint allows one to operate the AMB with a large bias flux, to obtain a desired bearing stiffness and force slew-rate, or with a very small (or even zero) bias flux for low-loss AMB operation. Experimental evidence is provided to illustrate the role of the flux bias in the control design and highlight the singularity issues associated with zero- and very low-bias AMB operation. Specifically, the tradeoff between bearing stiffness, power consumption, and power dissipation as a function of the bias is verified. Also, it is experimentally shown that the singularity issues present in the standard nonlinear backstepping control laws can be destabilizing in zero bias, and moreover, the newly developed CLF and passivity-based control laws effectively eliminate the zero-bias singularity issues.

Nomenclature

AMB active magnetic bearing
FWB flywheel battery
CMG control moment gyroscope
ESCMG energy storage control moment gyroscope
CFS constant flux sum
CFC complementary flux constraint
GCFC generalized complementary flux constraint
ZB zero-bias
LB low-bias
PMSM permanent magnet synchronous motor
IPACS Integrated Power and Attitude Control System

I. Introduction

The frictionless operation of the active magnetic bearing (AMB) has been taken advantage of in several industrial and scientific applications including vacuum pumps, hard disk drives, high-speed centrifuges

*Electrical Engineer, Space Vehicles Directorate, 3550 Aberdeen Ave, Kirtland AFB NM, 87117-5776, AIAA Member.
†Prof. Aerospace Engineering, Georgia Institute of Technology, Atlanta, GA 30332-0150, USA, AIAA Associate Fellow.
‡Prof. Electrical Engineering, Georgia Institute of Technology, Atlanta, GA 30332-0250, USA.

and turbines, artificial heart pumps, power quality conditioning, un-interruptible power supplies, magnetic catapults, high speed milling machines, magnetically levitated trains, etc.[1–5] In such applications, control algorithms are often employed to provide functionality that other types of bearing do not possess, such as compensation for rotor imbalance and/or rotor shaft flexibility. Several practical advantages, for instance the elimination of lubrication, vacuum operation, and the non-contacting nature, allow for low-maintenance, long life-span, high-speed bearings. In spite of the long list of benefits, AMBs do have some fundamental limitations including flux saturation, resulting in limited load capacity, and force slew-rate limits.

The primary interest of the aerospace community in AMBs is their application in flywheel batteries (FWBs) and advanced control moment gyroscopes (CMGs).[6] In a FWB, kinetic energy is stored in the rotating flywheel and converted back and forth to electrical energy using a motor/generator. FWBs have several advantages over the chemical batteries which are typically employed on spacecraft, such as long-life, large depth-of-discharge, a well-defined state-of-charge, and do not require constant or taper charging profiles.[7] Furthermore, FWBs may be designed[a] to compete with chemical batteries in terms of specific energy and typically outperform chemical batteries in terms of specific power. Advanced energy storage control moment gyroscopes (ESCMGs) that employ AMB-levitated rotors act as both a FWB and an attitude control actuator. These devices have been proposed to combine the functions of the attitude control and energy storage subsystems of satellites. Such an Integrated Power and Attitude Control System (IPACS) is projected to significantly reduce the satellite weight as well as double the mission lifespan.[6] Furthermore, ESCMGs are viewed as an enabling technology for space missions which require large attitude control torques and high pulse-power capability, such as Space Radar.[8,9]

Highly efficient FWBs require the use of *low-loss* AMBs. Although the use of a vacuum-operated AMB eliminates the mechanical losses in a FWB, electrical (magnetic core and Ohmic) and electromechanical (eddy-current drag) losses are often significant. Since each of these power loss mechanisms is proportional to the square of the electromagnet flux, it is imperative to minimize the flux required for rotor regulation to achieve a FWB with efficient energy storage capabilities.

Control design for an AMB is a two step process. The net force along an AMB control axis is $F = f_1 - f_2$, where f_1 and f_2 are the attractive (non-negative) forces from electromagnets 1 and 2 that compose the AMB control axis. The first step is to select an operational constraint between the electromagnets 1 and 2 so that for given a desired net force F, there exists a unique choice for f_1 and f_2. Once the constraint is determined, a stabilizing control law is constructed.

The customary constraint is called the constant-flux-sum[b] (CFS) constraint.[10] Using this constraint, a large flux bias is introduced into the electromagnets and the system is linearized about this operating point. Since power dissipation is proportional to the square of the flux, AMB and FWB power losses are minimized by operating the AMB with the smallest flux bias possible, ideally zero bias (ZB). However, the CFS biasing scheme results in an uncontrollable linearization in ZB. On other words, the AMB employing the CFS is linearly uncontrollable in ZB. Thus, one must avoid the customary biasing scheme when implementing low-loss AMBs.

One solution to this fundamental, zero-bias, linear controllability limitation is to use a nonlinear control scheme where opposing electromagnets of the AMB are activated in a complementary fashion. During operation, one electromagnet is turned off while the other is on and vice versa. Under this zero-bias *complementary flux constraint* (CFC), the AMB retains nonlinear controllability, but AMB performance may be sacrificed for low-loss operation, depending on the performance measure. For instance, bearing stiffness and force slew-rate are reduced as the bias flux is decreased.

Tsiotras and Wilson[11] propose a *generalized complementary flux constraint* (GCFC) for low-loss AMB operation. The GCFC is an extension of the CFC flux biasing scheme that allows one to operate an AMB with a large flux bias (to obtain a desired bearing stiffness and slew-rate) or with a very small bias (for low-loss AMB operation). In fact, using the GCFC one may reduce the bias all the way to zero[c] while retaining controllability, a feature that is absent from the standard CFS biasing technique. Issues related to the implementation of the GCFC are discussed in Refs. [12, 13]. Furthermore, this bias level may be changed on-line to meet possibly time-varying performance requirements. The AMB's performance under the influence of a given control law is evaluated in terms of closed-loop bearing stiffness, damping, force

[a]Flywheel batteries for spacecraft are designed to spin with maximum angular velocities on the order of $60 - 100$ krpm.

[b]When current is used to represent the electromagnet state, this constraint is called the constant-current-sum (ccs) constraint.[10]

[c]In this case, the GCFC corresponds to the CFC.

slew-rate, power consumption[d], and power dissipation. Experimental testing, presented in Section V-B, illustrates the relationship between the bias flux level and the various performance measures.

The low bearing stiffness implied by low-loss AMB operation introduces challenges into the control algorithm design. In particular, ZB operation leads to control law singularities when using voltage-mode amplifiers and standard nonlinear control design tools such as feedback linearization and integrator backstepping.[11,14–16] Typically, a control law singularity manifests itself as an infinite control voltage command. The control laws posed by Tsiotras and Wilson[11] , derived from the theory of dissipativity and control Lyapunov functions (CLF), effectively eliminate any singularity issues associated with voltage-mode, ZB and very low-bias (LB) operation. These control laws map from the state-space $(x, \dot{x}, \phi)$ to $\mathbb{R}$ $(u : \mathcal{D} \subseteq \mathbb{R}^3 \rightarrow \mathbb{R})$, where x is the rotor position, $\dot{x}$ is the rotor translational velocity, ϕ is a control flux, and u is the control law. It is shown that the singularity space -the space where the control law is not properly defined- for the standard nonlinear techniques is a plane in $\mathbb{R}^3$. The CLF control law reduces the singularity space to a line in $\mathbb{R}^3$ and the passivity-based technique eliminates the singularity altogether. This is significant because an infinite control signal results whenever the state trajectory intersects the singularity space. Experimental tests, presented in Section V-A, show that these "spikes" in the voltage command significantly degrade performance when employing backstepping for very LB and ZB operation. Furthermore, the CLF and passivity-based control laws perform significantly better than the backstepping law for LB and ZB and require less amplifier bandwidth to implement.

II. Dynamics and Energy Analysis of the FWB and the 1-DOF AMB

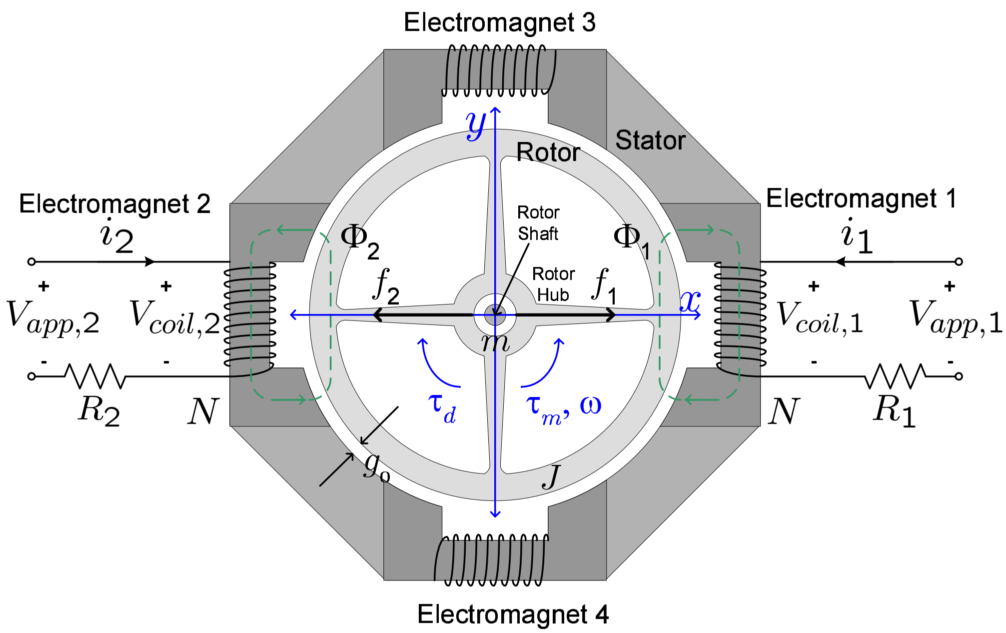

Figure 1. A two-dimensional schematic of the PREMAG magnetically suspended reaction wheel.

A two-dimensional schematic of the flywheel battery used in this investigation is shown in Figure 1. The rotor is regulated in the $x-y$ plane by electromagnets 1 through 4. When the rotor is centered in the $x-y$ plane the nominal airgap between the rotor and stator is g_0. Although omitted from the above schematic for clarity, four additional electromagnets, located directly beneath electromagnets 1 through 4, allow for control of the rotor tilt about the x and y axes. Although the full 6-DOF rotor control problem is worthy of study, this work ignores the rotor gyroscopic effects and instead focuses on the simpler control problem which assumes that four independent controllers can be designed to regulate the translational motion of the top and bottom of the rotor in the $x-y$ plane. Therefore, only the implementation of the GCFC and the control law verification on of one AMB control axes is presented. A passive bearing supports the rotor's weight in

[d]The power consumed is the power delivered to the electromagnet coil terminals. The power dissipated is the portion of the consumed power that is wasted in the AMB loss mechanisms.

the z direction (out of the page) and is omitted in this discussion. In this particular FWB configuration, the spin torque about the z axis is generated from a permanent magnet synchronous motor (PMSM) which is integrated into the interior of the rotor hub.

A. The FWB and 1-DOF AMB Model

The flywheel rotational dynamics are

$$J\dot{\omega} = \tau_m - \tau_d, \tag{1}$$

where J is the rotor rotational inertia about the spin axis, ω is the rotor angular velocity, τ_m is the torque applied by the spin motor, and τ_d is the electromagnetic drag torque. For $\omega \geq 0$, the PMSM acts as a motor when $\tau_m \geq 0$ and as a generator when $\tau_m < 0$. The electromagnetic drag torque, which results from eddy-current induction in the surface of the rotor, always opposes the rotor angular velocity and is[13, 17, 18]

$$\tau_d = pG\Phi^2\omega = k_d\omega, \tag{2}$$

where p is the number of electromagnets, G is a constant that depends on the AMB geometry and material properties, and Φ is the electromagnet flux. The drag coefficient k_d may be experimentally identified through rotor spin-down tests with $\tau_m = 0$.

Since the ratio of rotor the radius r to the nominal airgap g_0 is large, the customary "small airgap" assumption is made. Consequently, the electromagnet forces in the x and y direction are decoupled. Henceforth, only the x-axis, 1-DOF AMB dynamics are considered. The translational equation of motion is

$$m\ddot{x} = F = f_1 - f_2, \tag{3}$$

where m is the rotor mass, f_1 and f_2 are the electromagnet forces as illustrated in Figure 1, and F is the total electromagnet force on the rotor in the x direction.

The force from each electromagnet is[18, 19]

$$f_\mathrm{j} = \frac{\Phi_\mathrm{j}^2}{\mu_0 A_g}, \quad \mathrm{j} = 1, 2 \tag{4}$$

where Φ is the electromagnet flux, μ_0 is the permeability of free space, and A_g is the cross-sectional area of the airgap. Generally, the flux Φ is a nonlinear, multi-valued hysteresis function of the electromagnet current and the airgap: $\Phi = h(i, x)$. Under some mild presumptions, a technique exists for approximating this function using a lookup table: See the discussions in Refs. [12,13]. The function $h(i, x)$ that is produced from this approximation technique may be viewed as a flux estimator, valid for reconstruction of the flux from DC up to some bandwidth, in terms of the readily available position and current measurements. Using this technique, the effects of AMB flux saturation are incorporated into the model of $h(i, x)$; a property that other force-current-position relationships often neglect. The lookup table for one of the electromagnets is shown in Figure 2.

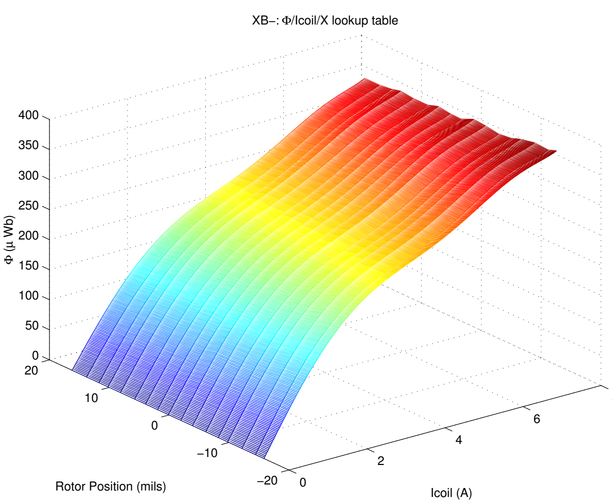

Figure 2. Two-dimensional lookup table relating the measured electromagnet current $i(A)$ and measured rotor position $x\,(\mathrm{mils})$ to the electromagnet flux $\Phi = h(i, x)\,(\mu\mathrm{Wb})$.

The electromagnet coils in Figure 1 are represented by zero-resistance coils (i.e. ideal coils) and a resistor R to account for the distributed winding resistance. Faraday's law relates the rate of change of coil flux to the voltage across the ideal coil: $N\dot{\Phi} = V_\mathrm{coil}$. Kirchhoff's voltage law relates the ideal coil voltage to the terminal coil voltage V_app. Using these principles, the resulting electrical dynamics are

$$\begin{aligned} V_\mathrm{app,j} &= i_\mathrm{j}R + V_\mathrm{coil,j} \\ &= i_\mathrm{j}R + N\dot{\Phi}_\mathrm{j}, \quad \mathrm{j} = 1, 2 \end{aligned} \tag{5}$$

where i is the coil current. In this study, voltage-mode amplifiers are used to drive the electromagnet coils.

Remark 1. *(current-mode vs. voltage-mode amplifiers)*
Electromagnet coils are typically driven by power servo amplifiers configured to operate in current mode or voltage mode. In current mode, feedback internal to the servo amplifier is used to make the coil current track a reference current. In voltage mode, feedback internal to the servo amplifier is used to make the voltage $V_{\rm app}$ in equation (5) track a reference voltage $V_{\rm r}$. The transfer function of $V_{\rm app}/V_{\rm r}$ typically resembles a low-pass filter with several hundred Hertz bandwidth.

B. Energy and Loss Analysis of the FWB and 1-DOF AMB

Energy is stored in the flywheel battery in the form of kinetic energy: $\mathcal{K} = \frac{1}{2}J\omega^2$. Using $\dot{\mathcal{K}} = J\omega\dot{\omega}$ and the flywheel equation of motion (1), the FWB energy storage dynamics are

$$\begin{aligned}\dot{\mathcal{K}} &= J\dot{\omega}\omega = \tau_m\omega - \tau_d\omega \\ &= \tau_m\omega - k_d\omega^2 \\ &= \tau_m\omega - \tilde{k_d}\frac{J}{2}\omega^2 \\ &= -\tilde{k_d}\mathcal{K} + \tau_m\omega, \end{aligned} \tag{6}$$

where $\tilde{k_d} = 2k_d/J$. Without loss of generality, the angular velocity is assumed to be non-negative. When acting as a motor, the electrical energy at the input terminals of the PMSM is converted to mechanical power, $\tau_m\omega$ is positive, and the mechanical energy stored in the flywheel increases. When acting as a generator, mechanical energy stored in the flywheel is converted to electrical power available at the PMSM's terminals, $\tau_m\omega$ is negative, and the mechanical energy stored in the flywheel decreases. The electromagnetic drag torque introduces a stable, first order pole into the energy storage dynamics. Thus, even when drawing no electrical power in generator mode ($\tau_m = 0$) from the flywheel, the "charge" stored in the flywheel battery will exponentially decay to zero with time constant $1/k_d$. Ideally, if $k_d = 0$, the energy storage dynamics are lossless and all of the input power is stored indefinitely in the FWB. Assuming that k_d is proportional to Φ_0^2 (see Remark (2)) it is imperative to minimize Φ_0 in the control design, ideally to zero, to maximize the FWB energy storage efficiency.

In addition to eddy-current drag losses in the FWB, there are losses associated with the operation of the electromagnets. Energy conversion from the AMB electrical input power to the mechanical force that produces rotor translation takes place in the magnetic field of the AMB coil. The dynamics of the magnetic field energy storage along the x control axis are[18, 19]

$$\dot{E}_{\rm fld,j} = -f_{\rm j}\dot{x}_{\rm j} + V_{\rm app,j}i_{\rm j} - i_{\rm j}^2R - p_{\rm core,j}, \qquad {\rm j} = 1, 2 \tag{7}$$

where $E_{\rm fld}$ is the energy stored in the electromagnet magnetic field, $f\dot{x}$ is the translational mechanical output power, $V_{\rm app}i$ is the applied electrical input power, i^2R is the Ohmic loss, and $p_{\rm core}$ represents the losses in the electromagnetic core due to eddy-current generation and hysteresis. Observe that a portion of the power supplied to (or consumed by) the bearing $V_{\rm app}i$ is converted into useful mechanical output power $f\dot{x}$ and the rest is dissipated (i.e. wasted) as heat in the Ohmic and core loss mechanisms. Since the AMB Ohmic and core loss are proportional to Φ^2, it is imperative to minimize the flux required for rotor regulation to minimize the energy dissipation in the AMB and maximize the AMB efficiency (i.e. the ratio of mechanical output power to electrical input power).

Table 1. Summary of FWB and AMB power losses.[18–20]

Power Loss	Proportional to
Ohmic loss in coil	$\propto \Phi^2,\ i^2R$
eddy-current loss in core	$\propto \Phi_{\rm max}^2$
hysteresis loss in core	$\propto \Phi_{\rm max}^{1.5-2.5}$
eddy-current drag loss	$\propto p, \Phi^2, \omega^2$

Remark 2. *(Low-Loss FWB and AMB operation)*
The FWB and AMB power loss mechanisms are summarized in Table 1. The instantaneous power loss in

each mechanism is proportional to the square of the magnetic flux. Since the flux is time-varying, one may minimize the rms power losses in both the FWB and the AMB by minimizing the rms value of the flux required to operate the AMB. When employing control designs that introduce a flux bias– for example, let $\Phi_{\rm j} = \Phi_0 + \phi_{\rm j}$ where $\Phi_{\rm j}$ is the total electromagnet flux, Φ_0 is the constant flux bias, and $\phi_{\rm j}$ is the control flux in the j^{th} electromagnet – the flux bias Φ_0 should be minimized to reduce the wasteful energy dissipation in the AMB and FWB.

III. AMB Flux Biasing and Performance Measures

Integral to every AMB control design is the selection of an operating constraint between the electromagnets that compose an AMB control axis. Since the total force along the x-axis, for example, is $F = f_1 - f_2$, there exist an infinite number of non-negative (electromagnet forces are always attractive) choices of f_1 and f_2 to realize a given desired total force $F_{\rm des}$. Thus, the AMB designer must supply a constraint equation between f_1 and f_2 to uniquely determine f_1 and f_2 for a given total force, $F_{\rm des}$. Typically, these force constraints are indirectly imposed through a constraint applied to the electromagnet voltage, current, or flux.[10] To illustrate the limitations of the standard biasing scheme for use with low-loss AMBs, the constant-flux-sum (CFS) constraint is first discussed. Next the generalized complementary flux constraint (GCFC) and the voltage switching law that implements it are introduced. Section III-D discusses the effect of the bias level on AMB performance measures such as, static load capacity, force slew-rate, closed-loop bearing stiffness and damping.

A. The Constant-Flux-Sum (CFS) Constraint

This constraint introduces a constant flux bias Φ_0 into the electromagnets so that $\Phi_1 = \Phi_0 + \phi_1$ and $\Phi_2 = \Phi_0 + \phi_2$. Since the electromagnet force depends on the square of the flux, the sign of the flux is immaterial. However, the fluxes are implemented so that Φ_1 and Φ_2 are always non-negative. The CFS constraint is imposed so that the sum of the total fluxes at all times is constant: $\Phi_1 + \Phi_2 = 2\Phi_0$. This implies that $\phi_1 = -\phi_2$. Conveniently, the two control fluxes ϕ_1 and ϕ_2 reduce to one by defining $\phi = \phi_1 = -\phi_2$. The control flux ϕ produces a net force in a differential manner:

$$\Phi_1 = \Phi_0 + \phi \tag{8a}$$
$$\Phi_2 = \Phi_0 - \phi, \tag{8b}$$

with the corollary constraint $|\phi| \leq \Phi_0$ so that $\Phi_{\rm j}$ is non-negative for $\mathrm{j} = 1, 2$.

The main advantage of the CFS is that it exactly linearizes the AMB translational dynamics permitting implementation of simple linear control algorithms in terms of ϕ as the control input. Imposing (8) on the translational equation of motion (3), one obtains

$$\begin{aligned} m\ddot{x} = F &= \frac{1}{\mu_0 A_g}[\Phi_1^2 - \Phi_2^2] \\ &= \frac{1}{\mu_0 A_g}\left[(\Phi_0 + \phi)^2 - (\Phi_0 - \phi)^2\right] \\ &= \frac{4\Phi_0}{\mu_0 A_g}\phi, \quad |\phi| < \Phi_0. \end{aligned} \tag{9}$$

Since low-loss operation is desirable, Φ_0 should be reduced ideally to zero. However, as Φ_0 tends towards zero in equation (9), the total electromagnet force becomes zero resulting in an uncontrollable system. In addition, reduction of Φ_0 to a small but non-zero value is detrimental to the AMB performance because the control flux is saturated $|\phi| < \Phi_0$. Thus, the main advantage of the CFS technique, namely the exact linearization property, is nullified by the absence of linear controllability under low-loss conditions. Consequently, the CFS constraint is a poor design choice for low-loss AMB operation.

B. Complementary Flux Constraints

The generalized complementary flux condition (GCFC) also introduces a flux bias ($\Phi_{\rm j} = \Phi_0 + \phi_{\rm j}$, $\mathrm{j} = 1, 2$), however, the control fluxes are constrained such that $\phi_1\phi_2 = 0$. Thus, at any given time, one of the control fluxes is zero while the other is adding to the bias flux to create a net force. For convenience, introduce the *generalized control flux*

$$\phi := \phi_1 - \phi_2. \tag{10}$$

The GCFC constraint written in terms of ϕ is

$$\begin{aligned} \phi_1 = \phi, \quad \phi_2 = 0 \quad \text{when} \quad \phi \geq 0 \\ \phi_1 = 0, \quad \phi_2 = -\phi \quad \text{when} \quad \phi < 0, \end{aligned} \tag{11}$$

and is imposed by following voltage-switching rule[11]

$$\begin{aligned} V_{\mathrm{c1}} = v, \quad V_{\mathrm{c2}} = 0 \quad \text{when} \quad \phi \geq 0 \\ V_{\mathrm{c1}} = 0, \quad V_{\mathrm{c2}} = -v \quad \text{when} \quad \phi < 0, \end{aligned} \tag{12}$$

where V_{cj} are the voltage reference inputs to the voltage-mode amplifiers and v is the *generalized control voltage* such that the electrical dynamics of equation (5) reduce to

$$\dot{\phi} = \frac{v}{N}. \tag{13}$$

For simplicity, the resistance has been neglected. Alternatively, one may redefine the control input by letting $v = V_{\mathrm{app}} - iR$ to cancel the resistance.

Imposing this flux constraint on the translational dynamics, (3) one obtains

$$\begin{aligned} m\ddot{x} = F &= \frac{1}{\mu_0 A_g}(\Phi_1^2 - \Phi_2^2) \\ &= \frac{1}{\mu_0 A_g}[\phi_1^2 - \phi_2^2 + 2\Phi_0(\phi_1 - \phi_2)] \\ &= \frac{1}{\mu_0 A_g}(2\Phi_0\phi + \phi|\phi|). \end{aligned} \tag{14}$$

Due to the presence of the $\phi|\phi|$ term in equation (14), the AMB retains its controllability properties as Φ_0 reduces to zero. In this case, the control fluxes are equal to the total fluxes $\phi_{\mathrm{j}} = \Phi_{\mathrm{j}}$ for $\mathrm{j} = 1, 2$, and the generalized control flux is $\phi = \Phi_1 - \Phi_2$. Consequently, the GCFC implements the standard CFC (see Ref. [11]) as a special case when the bias flux is zero.

C. GCFC Implementation

The GCFC implementation requires three components: (1) the ability to estimate the electromagnet flux, including its DC component, (2) the ability to synthesize a constant bias flux in the presence of a changing airgap, and (3) the implementation of the state-dependent, voltage-switching rule of equation (12). The lookup table, illustrated in Figure 2, satisfies requirement (1). Since the flux is a function of the electromagnet current and airgap, requirement (2) suggests that feedback, which modulates the current, is required to realize a constant bias flux in the presence of a changing airgap. The voltage switching rule of equation (12) is used to distribute the generalized control voltage v to the appropriate electromagnet depending on the sign of the generalized control flux ϕ. Thus, significant filtering of the position and current measurements is required to obtain clean flux measurements to avoid spurious switchings. A detailed presentation of the issues involved in the construction of the flux-lookup table and the implementation the GCFC is given in Refs. [12, 13].

Figure 3 shows the GCFC and control law implementation block diagram for the x control axis of the PREMAG reaction wheel. The electromagnet coils are driven by Copley Controls model 412 PWM voltage-mode servo-amplifiers. The amplifiers force the electromagnet terminal voltage $V_{\mathrm{app,j}}$ to follow the reference voltage $V_{\mathrm{r,j}}$ for $\mathrm{j} = 1, 2$. The transfer function of $V_{\mathrm{app}}/V_{\mathrm{r}}$ is a low-pass filter with a 200 Hz bandwidth. Since the electromagnet coils are linear in the voltage input, one may use superposition to independently realize a bias flux and control flux. In light of this, each reference voltage $V_{\mathrm{r,j}}$ is decomposed into a component that implements the flux bias $V_{\mathrm{b,j}}$ and a component that implements the control law $V_{\mathrm{c,j}}$:

$$V_{\mathrm{r,j}} = V_{\mathrm{b,j}} + V_{\mathrm{c,j}}, \qquad \mathrm{j} = 1, 2 \tag{15}$$

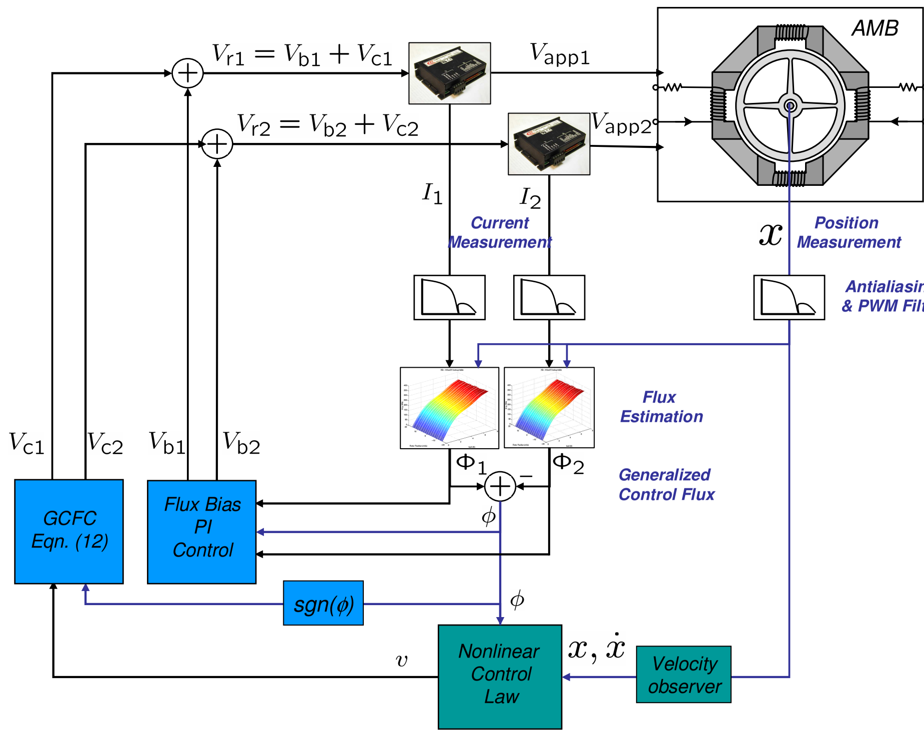

Figure 3. Block diagram for the implementation of the GCFC constraint and the control law.

The filtered current and position measurements are passed through the flux-lookup tables to produce estimates for Φ_1 and Φ_2. Subtracting these signals gives the generalized control flux ϕ. Given Φ_1, Φ_2, and ϕ, one can adjust $V_{\mathrm{b,j}}$ to drive the DC component of Φ_1 and Φ_2 to a desired flux bias level $\Phi_{0,\mathrm{des}}$. The nonlinear control law is constructed to stabilize equations (13) and (14) with the states x, $\dot{x}$, and ϕ. The control voltage v produced by the controller is distributed to the proper electromagnet $V_{\mathrm{c,j}}$ through the GCFC voltage switching rule of equation (12). Figure 4 illustrates the implementation of the GCFC with $\Phi_0 = 100\,\mu Wb$. For simplicity, the rotor position is uncontrolled and a sinusoidal generalized control voltage v is used.

D. AMB Performance Measures

Closed-loop AMB performance[21,22] is often characterized in terms of static load capacity, bearing stiffness, and force slew-rate. Such characterizations, which arise from the field of rotordynamics, facilitate an analogy where the AMB-levitated rotor under closed-loop control behaves similarly to a rotor on conventional bearings with a given spring stiffness and damping.[23]

The AMB static load capacity is a measure of the peak force that the bearing can produce. For any electromagnet, the maximum force is given by $F_{\max} = \Phi^2_{\mathrm{sat}}/\mu_0 A_g$, where Φ_{sat} is the value of the flux that saturates the electromagnet core. This is determined by the saturation flux density B_{sat} of the electromagnetic core material and the cross-sectional area A_p of the electromagnet pole: $\Phi_{\mathrm{sat}} = B_{\mathrm{sat}} A_p$. For common electromagnet core materials, $B_{\mathrm{sat}} \in [0.6 - 2.0]$ Tesla. When employing the GCFC constraint, the AMB static load capacity is limited

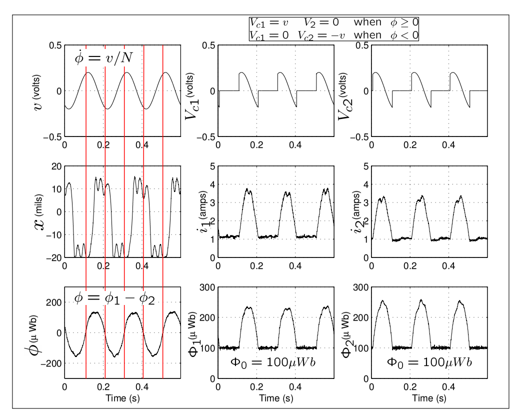

Figure 4. Open-loop GCFC implementation with sinusoidal control voltage v: $\Phi_0 = 100\mu Wb$.

only by the saturation flux density. Thus, the GCFC static load capacity is $F_{\text{GCFC}} = F_{\max}$. On the other hand, the largest force that the CFS constrained AMB can produce is $F_{\text{CFS}} = (2\Phi_0)^2/\mu_0 A_g$. Consequently, if $\Phi_0 < \Phi_{\text{sat}}/2$, then $F_{\text{CFS}} < F_{\max}$. In this case, the CFS scheme artificially limits the static load capacity of the AMB to less than the capacity of the electromagnets.

The force slew-rate measures the rate-of-change of the force with time. The time derivative of the force using equation (13) is

$$\dot{F}(\phi) = \frac{dF}{d\phi}\dot{\phi} = \frac{dF}{d\phi}\frac{v}{N} \leq \frac{dF}{d\phi}\frac{V_{\text{sat}}}{N} \tag{16}$$

where the control voltage is assumed to be less than the amplifier supply voltage: $v \leq V_{\text{sat}}$. This measure is related to the amplifier bandwidth.

Closed-loop bearing stiffness and damping measure the rate-of-change of the force with respect to the rotor position and velocity, respectively. These concepts are illuminated by assuming that the control flux is designed with position and velocity feedback: $\phi = \phi(x, \dot{x})$. Using the Taylor series expansion on the net force in the resulting closed-loop equation of motion, $m\ddot{x} = F(\phi(x, \dot{x}))$, gives

$$\begin{aligned} m\ddot{x} &\approx \frac{dF}{dx}\tilde{x} + \frac{dF}{d\dot{x}}\dot{\tilde{x}} \\ &= \frac{dF}{d\phi}\frac{d\phi}{dx}\tilde{x} + \frac{dF}{d\phi}\frac{d\phi}{d\dot{x}}\dot{\tilde{x}} \\ &= K(\phi)\tilde{x} + D(\phi)\dot{\tilde{x}} \end{aligned} \tag{17}$$

where the tilde is used to represent the deviation from the expansion point. One identifies the possibly nonlinear stiffness $K(\phi)$ and damping $D(\phi)$ terms from equation (17).

It is clear from equation (16) and (17) that the force slew-rate, the bearing stiffness, and damping each depend on the slope of the force-flux characteristic, $\frac{dF}{d\phi}$. Equations (9) and (14) show that $\frac{d}{d\phi}F_{\text{CFS}} = 4\Phi_0/(\mu_0 A_g)$ and $\frac{d}{d\phi}F_{\text{GCFC}} = 2(\Phi_0 + |\phi|)/(\mu_0 A_g)$ are linearly proportional to the bias flux. Thus, in both the CFS and GCFC schemes, a large bias flux enhances the bearing stiffness and force slew-rate. In addition, as the bias approaches zero, the bearing stiffness and force slew-rate decrease in both CFS and GCFC schemes, however, the CFS becomes uncontrollable while the GCFC maintains nonlinear controllability.

Heuristically, one expects a bearing with a large force slew-rate and bearing stiffness to be more "responsive" and have better disturbance rejection capabilities. The low-loss AMB has opposing performance measures: a LB design is desirable for efficient FWB energy storage and AMB operation, however, at the expense of decreased bearing stiffness, damping, and force slew-rate. Depending on the requirements of the application, this trade-off may or may not be debilitating. For example, terrestrial or ground vehicle energy storage applications may need to float the FWB rotor in the presence of large external disturbances and thus require large bearing stiffness. In a satellite attitude control application on the other hand, the rotor imbalance of the ESCMG itself may be a major source of attitude pointing error. In this case, it may be beneficial to have a low bearing stiffness to reduce the transmission of the rotor imbalance to the spacecraft and its sensing instruments. Thus, understanding of the effect of the bias level on the energy storage efficiency and the controller performance (with respect to the application requirements) is an important issue when using the GCFC.

IV. Control Design for the 1-DOF AMB

Assuming a constant bias is realized, the GCFC constrains the operation of the electromagnets so that the dynamics of the generalized control flux $\dot{\phi}$ (equation (13)) captures the dynamics of both electromagnets $\dot{\Phi}_1$ and $\dot{\Phi}_2$ (equation (5)). Thus the GCFC-constrained AMB, originally represented by the fourth order dynamic system (3)-(5), reduces to the third order dynamic system (14)-(13).

In order to work with a system having the minimum number of parameters, it is convenient to introduce the following non-dimensionalized state and control variables along with a non-dimensionalized time

$$\begin{gathered} x_1 := \frac{x}{g_0}, \quad x_2 := \frac{\dot{x}}{\Phi_{\text{sat}}\sqrt{g_0/\kappa}}, \quad x_3 := \frac{\phi}{\Phi_{\text{sat}}}, \\ u := \frac{v\sqrt{g_0\kappa}}{N\Phi_{\text{sat}}^2}, \quad \tau := t\frac{\Phi_{\text{sat}}}{\sqrt{g_0\kappa}} \end{gathered} \tag{18}$$

where $\kappa := m\mu_0 A_g$ and Φ_{sat} is the value of the saturation flux: See discussion in Section III-D.

In terms of these non-dimensionalized variables, the gcfc constrained dynamics (14)-(13) can be written in state-space form as follows

$$\begin{aligned} x_1' &= x_2 && \text{(19a)} \\ x_2' &= \epsilon x_3 + x_3|x_3| := f_2(x_3) && \text{(19b)} \\ x_3' &= u && \text{(19c)} \end{aligned}$$

where $\epsilon := 2\Phi_0/\Phi_{\text{sat}}$ and where prime denotes differentiation with respect to τ. Low-bias operation in this context therefore implies that $\epsilon \ll 1$, while zero bias implies that $\epsilon = 0$. The control law is computed for this system and re-dimensionalized before being applied to system (3)-(5). Note that the state equation (19) may be written in the standard control affine form $\dot{x} = f(x) + g(x)u$ with

$$f(x) = \begin{bmatrix} x_2 \\ f_2(x_3) \\ 0 \end{bmatrix}, \qquad g = \begin{bmatrix} 0 \\ 0 \\ 1 \end{bmatrix}. \tag{20}$$

Remark 3. *(Control Objectives)*
The control objective can be stated as follows: find a control law $u : \mathcal{D} \subseteq \mathbb{R}^3 \to \mathbb{R}$ such that

(i) the closed-loop system has an isolated equilibrium at the origin

(ii) the origin is asymptotically stable for all $x(0) \in \mathcal{D}$

(iii) The domain of definition $\mathcal{D} \subseteq \mathbb{R}^3$ of the control law $u(x)$ is as large as possible

A. Control Design via Backstepping

A common technique for the stabilization of cascaded systems is backstepping. In this approach, one views the state-variable x_3 as the control input to the mechanical dynamics (19a)-(19b) through $f_2(x_3)$. For convenience, let the state of the mechanical dynamics be $z = [x_1,\ x_2]^T$. One then assigns the dynamics for x_3 via the integrator (19c). To this end, first note that if one chooses x_3 such that

$$f_2(x_3) = \sigma(z) := -k_1 z_1 - k_2 z_2 \tag{21}$$

the z-subsystem is feedback linearized. In this case, the z-subsystem is given by $\dot{z} = Az$ where

$$A := \begin{bmatrix} 0 & 1 \\ -k_1 & -k_2 \end{bmatrix} \tag{22}$$

For $k_1 > 0$ and $k_2 > 0$ the matrix A is Hurwitz. Now introduce the function $u_0 : \mathbb{R}^2 \to \mathbb{R}$ such that $f_2(u_0(z)) = \sigma(z)$ for all $z \in \mathbb{R}^2$. It can be easily verified that

$$u_0(z) := -\frac{1}{2}\text{sgn}(\sigma(z))(\epsilon - \sqrt{\epsilon^2 + 4|\sigma(z)|}). \tag{23}$$

For $\epsilon = 0$ this function reduces to

$$u_0(z) = \text{sgn}(\sigma)|\sigma|^{\frac{1}{2}}. \tag{24}$$

If one now tries to implement the *virtual control law* $u_0(z)$ via (19c) one immediately faces the problem of the non-Lipschitz continuity of the inverse of the function $f_2(x_3)$ at the origin when $\epsilon = 0$. If, for instance, as usual one defines the error variable $\eta = f_2(x_3) - \sigma(z)$ one ends up with the backstepping control law

$$u(z, y) = \left(\frac{\partial f_2}{\partial x_3}\right)^{-1}\left[\frac{\partial \sigma}{\partial z}(Az + b\eta) - 2b^T Pz - \gamma\eta\right], \quad \gamma > 0 \tag{25}$$

where $P > 0$ satisfies the matrix inequality (such a P always exists since A is Hurwitz) $A^T P + PA < 0$. With A as in equation (22), the closed-form solution of $A^T P + PA = -I_{2\times 2}$ for P is

$$P = \frac{1}{2}\begin{bmatrix} \frac{k_1^2 + k_1 + k_2^2}{k_1 k_2} & k_1 \\ k_1 & \frac{1+k_1}{k_1 k_2} \end{bmatrix}. \tag{26}$$

Using the Lyapunov function

$$V(z,y) = z^T P z + \frac{1}{2}\eta^2, \tag{27}$$

it can be easily shown that the control law (25) globally asymptotically stabilizes the system (19) for non-zero ϵ. However, the control law (25) is singular at $x_3 = 0$ for $\epsilon = 0$. Indeed, since

$$\left(\frac{\partial f_2}{\partial x_3}\right)^{-1} = \frac{1}{2|x_3| + \epsilon}, \tag{28}$$

the control law (25) is not defined at $x_3 = 0$ for the case of zero-bias flux. The singularity space (i.e. the set where u is undefined) is a plane in $\mathbb{R}^3$. An infinite voltage command is issued whenever the system trajectory crosses the plane of singularity. Thus, in ZB operation, control law (25) renders the origin of (19) asymptotically stable for all initial conditions $x_0 \in \mathcal{D}_1 = \{x \in \mathbb{R}^3 | \ x_3 \neq 0\}$.

It should come as no surprise that the singularity is still present even if one introduces an alternative definition for the error. For example, let $\eta = x_3 - u_0(z)$ the z-subsystem can be written as

$$\dot{z} = Az + b(z, x_3)\eta \tag{29}$$

where $b(z, x_3) = [0, \ \pi(z,y)]^T$, and where $\pi(z, x_3) \in \mathcal{C}^0$ satisfies $f_2(x_3) = f_2(u_0(z)) + \pi(z, x_3)\eta$. For example, one may choose[e]

$$\pi(z, x_3) := \frac{f_2(x_3) - f_2(u_0(z))}{x_3 - u_0(z)}. \tag{30}$$

Using the same Lyapunov function candidate as in (27) it can be shown that the choice of the control law

$$\begin{aligned} u(z, x_3) = &\frac{1}{\sqrt{\epsilon^2 + 4|\sigma(z)|}} \left(\frac{\partial \sigma}{\partial z}\right) \Big(Az + b(z, x_3)\eta\Big) \\ &- 2b^T(z, x_3)Pz - \gamma\eta, \qquad \gamma > 0 \end{aligned} \tag{31}$$

results in a globally asymptotically closed-loop system for all $\epsilon \neq 0$. The control law (31) is bounded for all $\epsilon > 0$. For $\epsilon = 0$ this control law exhibits a singularity when $\sigma(z) = 0$, and hence, renders the origin of (19) asymptotically stable for all $x_0 \in \mathcal{D}_2 = \{x \in \mathbb{R}^3 | \ \sigma(z) \neq 0\}$ in zero-bias operation.

B. Control Design via Control Lyapunov Functions (CLF)

Control Lyapunov function (CLF) design is useful for systems with cascaded structures and is closely related to backstepping.

Definition 1. *A function $V : \mathbb{R}^n \to \mathbb{R}_+$ is a control Lyapunov function (CLF) for the system $\dot{x} = f(x) + g(x)u$ if it satisfies the following properties:*

(i) *V is positive definite*

(ii) $V \in \mathcal{C}^1$

(iii) *V is radially unbounded, and*

(iv) $L_f V(x) < 0$ *for all* $x \neq 0$ *such that* $L_g V(x) = 0$

where the lie derivative is $L_f V(x) :=< \nabla_x V(x), f(x) >$ for vector field f and scalar function V.

The system $\dot{x} = f(x) + g(x)u$ is stable when $\dot{V}(x) = L_f V(x) + L_g V(x)u < 0$ for all non-zero x. To satisfy this inequality, one chooses u to dominate Ł$_f V(x)$ so that $\dot{V} < 0$. CLF property (iv) guarantees that this inequality holds even when one looses controllability at $L_g V(x) = 0$.

To relate the CLF concept to cascaded systems and the backstepping discussion in the previous section, suppose that $u_0(z)$ stabilizes the mechanical z-subsystem dynamics with Lyapunov function $V_0(z) \in \mathcal{C}^1$. Then, by definition,

$$\dot{V}_0(z) = L_{[z_2, f_2(u_0(\sigma(z)))]^T} V_0(z) < 0, \quad \forall x \neq 0.$$

[e]Notice that $\pi(z, x_3) \in \mathcal{C}^0$ for all $\epsilon \geq 0$ since $f_2 \in \mathcal{C}^1$.

The function $V(z,\eta) = V_0(z) + \frac{1}{2}\eta^2$ with $\eta = x_3 - u_0(z)$ satisfies property (iv) of the CLF definition. Using the cascaded structure of the f and g in equation (20), $\dot{V}(x) = L_f V(x) + L_g V(x) u$ may be rewritten

$$\begin{aligned}
\dot{V}(z,\eta) &= L_f V(z,\eta) + L_g V(z,\eta) u \\
&=< [\frac{\partial V}{\partial z_1}, \frac{\partial V}{\partial z_2}, \frac{\partial V}{\partial \eta},], [z_2, f_2(x_3), 0]^T > + < [\frac{\partial V}{\partial z_1}, \frac{\partial V}{\partial z_2}, \frac{\partial V}{\partial \eta},], [0,0,1]^T > u \\
&= L_{[z_2, f_2(x_3)]} V_0(z) + \eta u \\
&= L_{[z_2, f_2(u_0(\sigma(z)))]} V_0(z) < 0, \qquad \text{for} \quad \eta = 0.
\end{aligned}$$

Thus, the Lyapunov function (27) used in the backstepping design is practically a CLF for (19), however, it fails the CLF smoothness property (ii): That is, $V(z,\eta) = V_0 + \frac{1}{2}\eta^2$ is not in $\mathcal{C}^1$ because $\frac{1}{2}\eta^2$ is not smooth enough. Indeed, given $\eta = x_3 - u_0(\sigma(z))$, then

$$\dot{\eta} = u - \frac{\partial u_0}{\partial \sigma}\frac{\partial \sigma}{\partial z}\dot{z}.$$

Since

$$\frac{\partial u_0}{\partial \sigma} = \frac{1}{\sqrt{\epsilon^2 + 4|\sigma(z)|}},$$

$\dot{\eta}$ is fails to be continuous at $\sigma(z) = 0$ in zero bias ($\epsilon = 0$).

Using the results from Ref. [24], one may introduce a new backstepping error function which is smooth enough to make V be a CLF. To this end, define the continuous function $\psi(z, x_3) \in \mathcal{C}^0$ so that it behaves like the backstepping error function: That is, $\psi(z, x_3) = 0$ implies that $x_3 = u_0(z)$. Now construct the differentiable function $\Psi(z, x_3) \in \mathcal{C}^1$

$$\Psi(z, x_3) := \int_0^{x_3} \psi(z, q) dq \tag{32}$$

where for all $z \in \mathbb{R}^2$, $\Psi(z, x_3) \to \infty$ as $|x_3| \to \infty$. The form of the CLF is then given by

$$V(z, x_3) = V_0(z) + \Psi(z, x_3) - \Psi(z, u_0(\sigma(z))). \tag{33}$$

Given the CLF in equation (33), one can derive a globally asymptotically stabilizing control law for equation (19).

Proposition 1. *(CLF control from Refs. [11, 13])*
Given the state equation (19), select the virtual control function $u_0(z)$ as in (23) to stabilize the mechanical z-subsystem dynamics with $V_0(z) = z^T P z$ and P as in equation (26). Next, let

$$\psi(z, x_3) = \epsilon(x_3 - u_0(z)) + x_3|x_3| - u_0(z)|u_0(z)|.$$

Then,

$$V(z, x_3) = \frac{\epsilon}{2}(x_3 - u_0)^2 + \frac{1}{3}|x_3|x_3^2 - x_3 u_0(z)|u_0(z)| + \frac{2}{3}|u_0(z)|u_0(z)^2 + V_0(z)$$

is a CLF for (19) and control law

$$\begin{aligned}
u(z, x_3) =& \psi(z, x_3)^{-1}\Big[(x_3 - u_0(z))(k_1 x_2 + k_2 f_2(x_3)) + \frac{\partial V_0}{\partial x_2}\Big(f_2(u_0(z) - f_2(x_3))\Big)\Big] \\
&- \gamma(x_3 - u_0(z)), \quad \gamma > 0
\end{aligned} \tag{34}$$

will globally asymptotically stabilize (19) for $\epsilon \neq 0$. For $\epsilon = 0$, (34) renders the origin of (19) asymptotically stable for all $x_0 \in \mathcal{D}_3 = \{x \in \mathbb{R}^3 |\ x_3 \neq 0\ \&\ \sigma(z) \neq 0\}$.

One may verify that the CLF control law (34) is singular in ZB when $x_3 = 0$ and $u_0(z) = 0$.

C. Control Design via Passivity

The control design via passivity again uses integrator backstepping to take advantage of the cascaded structure of the system. However, it uses a very simple virtual control law

$$u_0(z) = -k_1 z_1 - k_2 z_2 \tag{35}$$

with $k_1 > 0$, $k_2 > 0$, to globally asymptotically stabilize the z-subsystem dynamics. In contrast to the backstepping and CLF control laws, this virtual control law does not linearize the mechanical z-subsystem dynamics and the resulting closed-loop system is nonlinear. Consequently, the stability proof for the mechanical z-subsystem dynamics is more difficult. The proof takes advantage of the Mean-Value Theorem and ideas from dissipativity theory: See Refs. [11, 13] for a detailed discussion.

The main advantage of this passivity-based virtual control law is that it does not implement the inverse of the function $f_2(x_3)$. The singularity in each of the backstepping and CLF designs can be traced to the non-Lipschitz continuity of $f_2^{-1}(x_3)$. Consequently, the passivity-based virtual control law leads to a globally defined control law for (19), even in zero bias operation. The following proposition is taken directly from Refs. [11, 13].

Proposition 2. *(GAS via passivity and backstepping [11, 13])*
The system (19) with the control law

$$u = -k_1 z_2 - k_2 f_2(x_3) - z_2 \pi(z, x_3) - \gamma\eta \tag{36}$$

where k_1, k_2, γ are positive constants, $\eta = x_3 - u_0(z)$, $u_0(z)$ as in (35), and the continuous function $\pi(z, x_3)$ as in (30), is globally asymptotically stable (GAS).

Since the function $\pi(z, x_3)$ is continuous, the passivity-based control law (36) is defined for all $x \in \mathcal{D}_4 = \mathbb{R}^3$. That is, passivity-based control law is completely nonsingular, even in ZB operation ($\epsilon = 0$).

D. Control Law Singularities

Control objective (iii) listed Remark 3 states that the domain of definition of $u : \mathcal{D} \subseteq \mathbb{R}^3 \to \mathbb{R}$ should be as large as possible. Each of the control laws presented in Section IV are nonsingular for $\epsilon \neq 0$. However, the backstepping and CLF control laws are singular in ZB operation. Specifically, the singularity space (i.e. the complement of the domain of definition) of the backstepping control laws of equations (25) and (31) are $\overline{\mathcal{D}_1} = \{x \in \mathbb{R}^3 | \epsilon = 0 \ \& \ x_3 = 0\}$ and $\overline{\mathcal{D}_2} = \{x \in \mathbb{R}^3 | \epsilon = 0 \ \& \ k_1 z_1 + k_2 z_2 = 0\}$, respectively. These planes represent subspaces in $\mathbb{R}^3$, and hence, always have an intersection. In addition, the singularity space of (34) is $\overline{\mathcal{D}_3} = \{x \in \mathbb{R}^3 | \epsilon = 0 \ \& \ \ x_3 \neq 0 \ \& \ \sigma(z) \neq 0\}$. Since $\overline{\mathcal{D}_3} = \overline{\mathcal{D}_1} \cap \overline{\mathcal{D}_2}$, the CLF control law is a line in $\mathbb{R}^3$. Finally, the passivity based control law (36) is defined for all of $\mathbb{R}^3$.

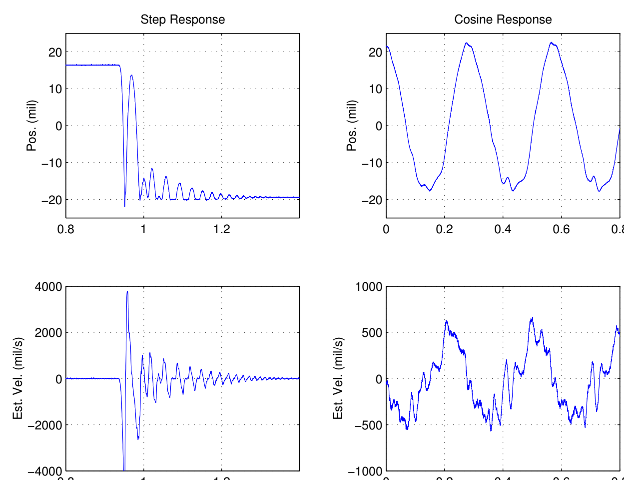

Figure 5. Velocity estimation for a step-like and cosine-like position input.

An infinite control voltage is requested whenever the state trajectory intersects the singularity space. Furthermore, one should expect the control voltage to become arbitrarily large as the state trajectory gets arbitrarily close to the singularity. Thus, unreasonably large control voltages may be generated from the backstepping and CLF control laws with very small but non-zero bias flux. Heuristically, one would additionally expect the large control "spikes" to occur more often from the backstepping controllers as compared to the CLF control law because it is "easier" for the state trajectory to encounter a planar singularity than a linear singularity in $\mathbb{R}^3$. Since the passivity-based control law is non-singular in zero-bias, it will always produce a bounded control input voltage.

E. Velocity Estimation

Since each control law assumes velocity feedback and only position and currents are measured, the velocity must be estimated. One could construct a nonlinear observer for the system, however a simpler approach is taken in this work. Since the closed-loop bandwidth of the AMB was expected to be on the order of 100 Hz, a gain-limited differentiation filter is implemented

$$\frac{V(s)}{x(s)} = \frac{(1+b)^2 s}{(s+b)^2}$$

where $b = 2\pi 200$. This filter approximates a derivative up to about 200 Hz and then rolls off the high-frequency gain at $-20\,\mathrm{dB/dec}$. The filter does introduce some extra phase shift within the AMB closed-loop bandwidth, but does not affect the control performance significantly. Figure 5 illustrates the velocity estimation for a step-like and cosine-like position input.

V. Experimental Validation

The control laws of Section IV were used to magnetically levitate the reaction wheel shown in Figure 1. The experiment is implemented using a dSPACE® DS1103 controller board sampling at 6.6 kHz and the accompanying MathWorks® and dSPACE® software: Matlab®, Simulink®, Real-Time Workshop®, and ControlDesk®. Each control law employs the GCFC using the block diagram in Figure 3: See Refs. [12, 13] for additional implementation details. The experimental data serves to verify two aspects of the control designs. The control law singularity analysis is verified in the following section and the behavior of the AMB with respect to the performance measures as a function of the bias flux is illustrated in Section V-B.

A. Experimental Validation of Control Law Singularity Analysis

Each control law from Section IV is found to stabilize the rotor with bounded control inputs when employing a large bias. However, when operating in zero-bias, the singular backstepping control law (equation (25) or (31)) may request an infinite control voltage. Moreover, when operating with a very small, but non-zero bias, the backstepping control laws often generate bounded, but unreasonably large control voltages. Although the CLF control law is nonsingular in ZB, it is found in practice that it rarely generates voltages of unreasonable magnitude.

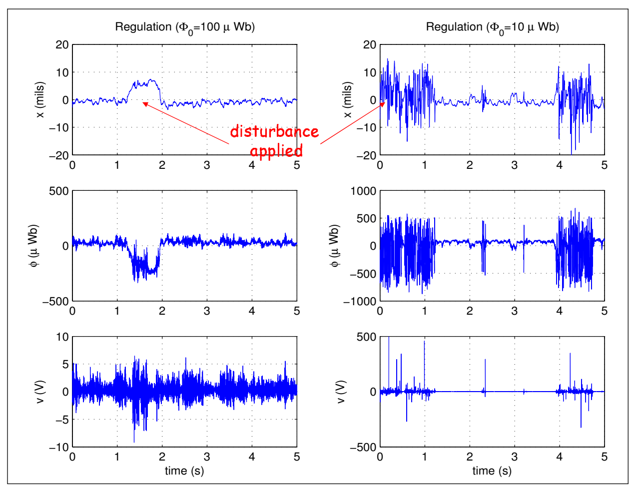

Figure 6. Backstepping control law (equation (31)): $k_1 = 2$, $k_2 = 2$, $\gamma = 0.5$. Regulation to $x = 0$ against disturbances for large bias $\Phi_0 = 100\,\mu\mathrm{Wb}$ (left column) and small bias $\Phi_0 = 10\,\mu\mathrm{Wb}$ (right column).

Figure 6 shows the rotor position x, the generalized control flux ϕ, and the generalized control voltage v for the backstepping control law (equation (31)). The left column shows large-bias operation $\Phi_0 = 100\,\mu\mathrm{Wb}$ whereas the right column shows very low-bias operation $\Phi_0 = 10\,\mu\mathrm{Wb}$. Under large-bias operation, the control law regulates the rotor to $x = 0$. At about 1.25 s, a large external disturbance is manually applied to the rotor (by physically pushing on the rotor). The AMB quickly recovers and resumes regulation to $x = 0$ when the rotor is released at about 2 s. Since the backstepping control law is nonsingular in large bias operation, the generalized control voltage v is bounded (less than about 10 V) during operation as expected.

AMB behavior typical of very low-bias backstepping control is shown in the right column of Figure 6. When operating with very low bias, the rotor regulation to $x = 0$ is unacceptable. At $t = 0$, a "impulse" disturbance is manually applied to the rotor (by tapping on the rotor). Intense vibration of the rotor ensues until about 1.25 s, followed by a brief period where the control law resumes regulation to $x = 0$. However, at about 4 s, another intense vibration occurs (even with no applied external disturbance); the rotor even bumps into the stator at $x = -g_0 = -20$ mils. Note that the intense rotor vibration corresponds to the presence of huge "spikes" in the generalized control voltage. Although the implemented control law is nonsingular ($\Phi_0 \neq 0$), the requested control voltage is unreasonably large (often thousands of volts in magnitude). The voltage "spikes" arise from the state trajectory intersecting the plane of singularity $\mathcal{D}_2$.

Recall that the Copley voltage-mode amplifiers try to make the coil voltage V_{app} follow V_{r}. These amplifiers have limited bandwidth and are powered from a 28 V power supply (typical of a spacecraft bus): $V_{\text{sat}} = 28$ V. In light of this, one may expect that the huge "spikes" in the requested control voltage in V_{r} will saturate and have little impact on the controller performance. This is clearly not the case, as shown in Figure 6.

The singularity behavior of the control laws may be further characterized by inspecting the frequency content of the generalized control voltage v. Figure 7 illustrates the zero-bias operation of the backstepping controller (25), the CLF controller (34), and the passivity-based controller (36) regulating the rotor to the origin in the presence of periodic disturbance (from the spinning rotor); control gains are given in the figure caption. The rms error is used as a measure of the control law regulation performance. One may consistently select control gains k_1, k_2, and γ so that the ZB passivity and CLF control laws achieve rotor regulation performance with $e_{\text{rms}} < 1 - 2$ mils. Note however that the backstepping control law (equation (25)) has trouble regulating the rotor to less than $e_{rms} = 4$ mils, even for larger k_1 and γ gains.

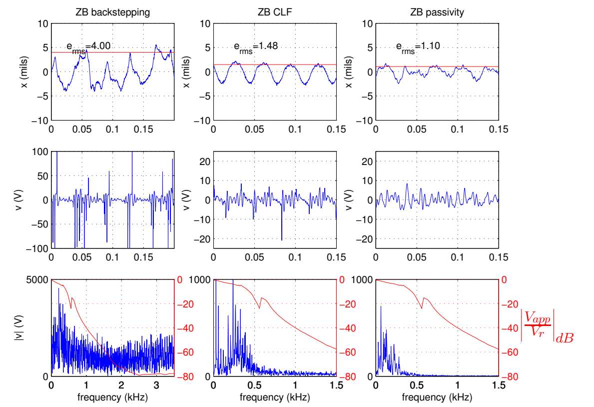

Figure 7. Column-wise comparison of the spectral content of the generalized control voltage v in ZB operation: (left) backstepping control equation (31) with $k_1 = 4$, $k_2 = 2$, and $\gamma = 0.5$; (middle) CLF control equation (34) with $k_1 = 1$, $k_2 = 0.5$, and $\gamma = 0.5$; (right) passivity control equation (36) with $k_1 = 6$, $k_2 = 2$, and $\gamma = 0.5$.

The middle row of Figure 7 shows the generalized control voltage for each control law. The ZB backstepping controller frequently generates voltage "spikes" that are thousands of volts in magnitude. The CLF control law is technically singular in ZB, however, it rarely generates large voltage "spikes" in practice. For instance, at 0.075 s, a voltage "spike" is generated, but it is only a modest 20 V. The relatively low rate-of-occurrence of voltage "spikes" in the CLF as compared to the backstepping control law is attributed to the fact that the singularity space of the CLF control law (a line in $\mathbb{R}^3$) is much smaller than the backstepping singularity space (a plane in $\mathbb{R}^3$). Thus, it is less likely that the state trajectory will intersect or come "close" to the CLF singularity space. Note that the passivity control law is well-behaved in ZB and has control voltage less than 10 V.

The last row of Figure 7 shows the frequency content of each control signal. The frequency content of the backstepping control law is much larger than that of the CLF control, while the frequency content of the passivity-based control has the smallest bandwidth. Superimposed over the spectral voltage content is the measured voltage-mode amplifier transfer function $\frac{V_{app}}{V_r}(s)$. Observe that the voltage-mode amplifier filters out a significant portion of the backstepping controller energy while the CLF and passivity-based control is applied to the electromagnet coils essentially unchanged. One concludes that control laws with a large singularity spaces demand voltage-mode amplifiers with an unreasonably large bandwidth to implement.

B. Experimental Validation of the Role of the AMB Bias Flux

As previously discussed in Section III-D, when using the GCFC it is important to understand the effect of the bias flux on the energy storage efficiency (electrical and electromechanical losses) and the controller performance (bearing stiffness, damping, etc.). Heuristically, one expects a bearing with large bias, and hence large bearing stiffness and damping, to be more "responsive" are possess good disturbance rejection capability. However, this is achieved at the cost of increased power consumption and power losses.

The influence of the bias flux on the AMB performance measures has been experimentally verified[13] for the for each control law in Section IV, however, only the observations on the passivity-based control law equation (36) are presented. The bias level has a similar effect on the performance measures of the AMB under CLF and backstepping control. However, when operating in zero bias, the performance of the backstepping controller is significantly degraded to the point that it is difficult to draw fair comparisons with the CLF and passivity ZB control laws.

Figure 8 shows the step response of the rotor using the passivity-based control law in equation (36) with gains $k_1 = 3$, $k_2 = 0.5$ and $\gamma = 0.5$. Position x, control flux ϕ, and control voltage v are shown for $\Phi_0 = 0$ μWb (left column) and for $\Phi_0 = 150$ μWb (right column). ZB operation results in a step response with ringing; a response typical of a bearing with little bearing stiffness and damping. On the other hand, the large bias results in fast response with no ringing; a response typical of a bearing with significant bearing stiffness and damping. Thus, when holding the control gains constant, the bias directly effects the bearing stiffness and damping as expected.

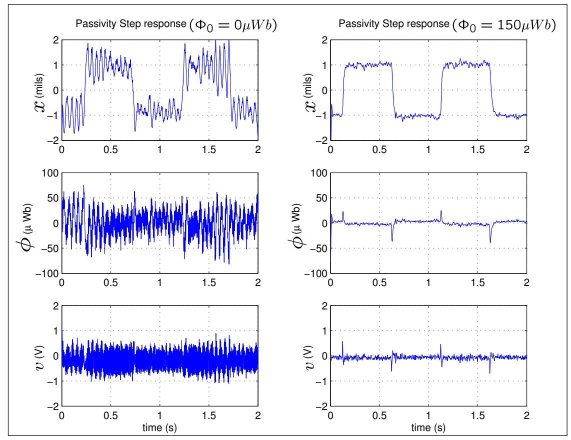

Figure 8. Step response of the rotor using the passivity-based control law in equation (36) with gains $k_1 = 3$, $k_2 = 0.5$ and $\gamma = 0.5$. Position x, control flux ϕ, and control voltage v are shown for $\Phi_0 = 0$ μWb (left column) and for $\Phi_0 = 150$ μWb (right column).

The rms power consumption and total square flux required for AMB rotor regulation are useful electrical performance measures. The power consumption of the AMB per control axis is computed from the measured coil voltage and current: $P_{\text{supp,rms}} = (V_{\text{app},1} i_1)_{\text{rms}} + (V_{\text{app},2} i_2)_{\text{rms}}$. Since the AMB and FWB instantaneous power losses are proportional to Φ^2, the rms value of the squared flux is used as a measure of the losses over time. That is, the AMB and FWB losses over time are gauged by the rms values of the total square flux $(\Phi_1^2)_{\text{rms}} + (\Phi_2^2)_{\text{rms}}$. Recall that the rms value of a signal is given by $x_{\text{rms}}(t) = \sqrt{\frac{1}{t}\int_0^t x(\tau) d\tau}$, and generally, $(\Phi^2)_{\text{rms}} \neq (\Phi_{\text{rms}})^2$.

Given any two control laws, or even the same control law with different bias levels, it is difficult to "match" their transient responses, and therefore difficult to draw a "fair" comparison of the control laws based on power consumption or total square flux usage. Although the qualitative observations made about the bearing stiffness and damping are appealing to the control engineer when looking at the familiar step response (such as those drawn about Figure 8), it is easier to obtain "fair" comparisons when operating the AMB under some steady-state behavior. A persistent periodic disturbance, similar to rotor imbalance, is applied to the rotor. As a result, the control law regulates the rotor to a desired position x_{des} with a roughly sinusoidal regulation error $e(t) = x_{\text{des}} - x(t)$. Two realizations of a control law are considered comparable if they can regulate the rotor to the desired set point with the same regulation performance, measured by the rms value of the regulation error, e_{rms}. Given two control law realizations with the same e_{rms} value, one may use the rms value of the control flux ϕ_{rms} to compare the amount of control effort. Furthermore, the rms value of the total flux squared maybe be related to the losses in the AMB and FWB. Figure 9 shows the calculation of such performance measures.

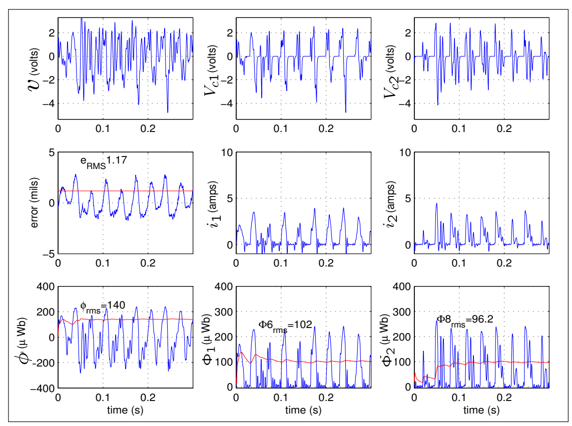

Figure 9. Steady-state rotor regulation against a periodic disturbance: Illustrated are the rms regulation error, the rms control flux, and the rms value of the total fluxes.

As discussed in Section IV-D, the bias should affect the bearing stiffness. From equation (17) and the passivity based virtual control law u_0 in equation (35), the nonlinear stiffness term is

$$K(\phi) = \frac{\partial F}{\partial \phi}\frac{\partial \phi}{\partial x_1} = \frac{2}{\mu_0 A_g}(\Phi_0 + |\phi|)k_1,$$

where k_1 behaves like a proportional gain. Thus, for a constant proportional gain k_1, the bearing stiffness should increase as Φ_0 increases, and the control effort should be less to obtain the same regulation performance. These ideas are illustrated in Figure 10.

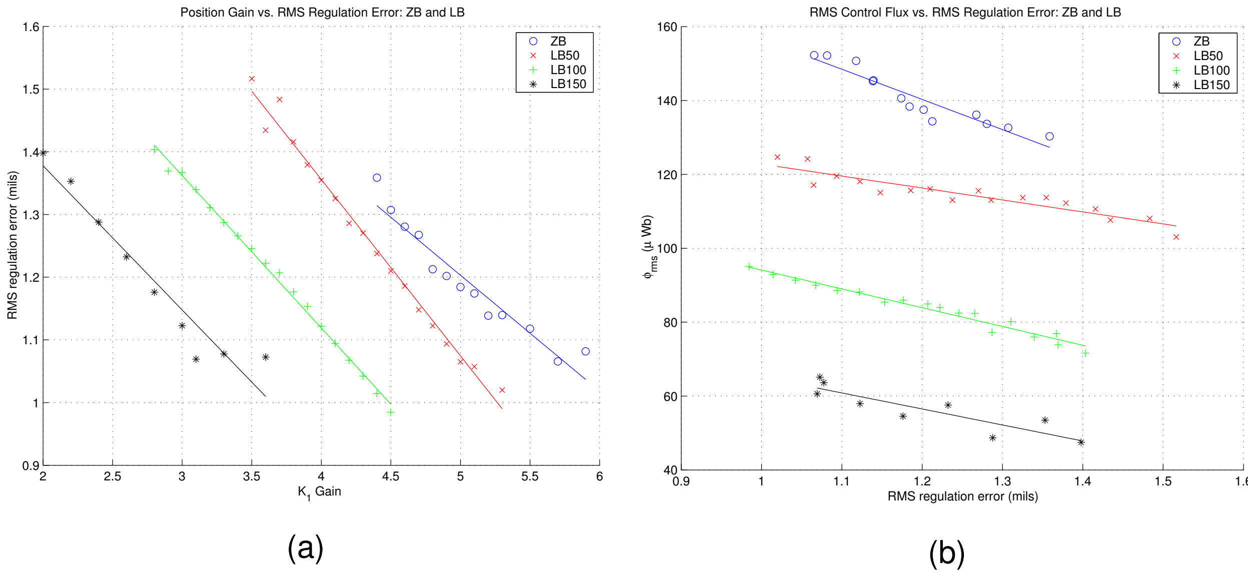

Figure 10. Bearing stiffness as a function of the bias flux using the passivity-based control law: (a) rms regulation error $e_{\rm rms}$ vs. "proportional" gain k_1. (b) rms control flux $\phi_{\rm rms}$ vs. rms regulation error $e_{\rm rms}$.

Figure 10a shows a parameter study of the passivity control law's regulation performance: the rms regulation error $e_{\rm rms}$ is plotted as a function of the proportional gain k_1 for several values of the bias flux; $\Phi_0 = 0$, 50, 100, and 150 μWb. For a given value of Φ_0, one obtains tighter regulation by increasing the proportional gain. Now, to obtain a given desired regulation performance $e_{\rm rms}$, one requires a smaller value of the proportional gain k_1 as the bias increases. This implies that the bearing stiffness increases as the bias increases, as predicted.

Figure 10b shows the rms value of the control flux $\phi_{\rm rms}$ as a measure of the control effort. The control effort $\phi_{\rm rms}$ is plotted vs. the regulation performance measure $e_{\rm rms}$ for several values of the bias. For a given value of Φ_0, one requires greater control effort to obtain tighter regulation tolerances. Now, to obtain a desired regulation performance $e_{\rm rms}$, the required $\phi_{\rm rms}$ decreases as the bias increases. In other words, less control effort is needed with increasing bias. This again suggests that the bearing stiffness increases with increasing bias flux.

Figure 11 illustrates the electrical performance measures. Figure 11a shows the total square rms flux and is a measure of the losses in the AMB and FWB. For a given Φ_0, more rms control flux $\phi_{\rm rms}$ and consequently, more total square flux $(\Phi_1^2)_{\rm rms} + (\Phi_2^2)_{\rm rms}$ is required to obtain tighter regulation tolerances. Since the AMB and FWB rms power losses are proportional to $(\Phi_1^2)_{\rm rms} + (\Phi_2^2)_{\rm rms}$, one incurs more power losses to regulate to tight error tolerances. To regulate the rotor with a given desired regulation performance $e_{\rm rms}$, the total square flux increases with increasing Φ_0. That is, the AMB and FWB losses increase with increasing Φ_0 as expected.

Figure 11b shows the rms power consumption $P_{\rm supp,rms} = (V_{\rm app,1} i_1)_{\rm rms} + (V_{\rm app,2} i_2)_{\rm rms}$ for the AMB vs. $e_{\rm rms}$. For a given Φ_0, more rms power is required to regulate the rotor to a tighter error tolerance. This agrees with intuition since the additional control effort costs additional power to implement. Notice however that for a given error tolerance $e_{\rm rms}$, one does not necessarily increase the power consumption when one increases the bias flux. For instance, for $e_{\rm rms} = 1.3$ mils, it takes the least power to operate in ZB. However, for $e_{\rm rms} = 1.3$ mils, it takes less power to operate the AMB with $\Phi_0 = 100\,\mu$Wb than it does to operate with $\Phi_0 = 50\,\mu$Wb. Furthermore, one sees that for $e_{\rm rms} < 1.1$ mils, it is more efficient to operate the AMB with $\Phi_0 = 100\,\mu$Wb than in ZB.

This behavior of the electrical performance measures can be understood by considering the effect of the bias flux on the bearing stiffness. As shown in Figure 10, for a given regulation error $e_{\rm rms}$, an increase in the bias flux results in a bearing stiffness increase and a decrease in the required control flux. In this situation, more power is required to implement the larger bearing stiffness Φ_0, however, less power is required to realize

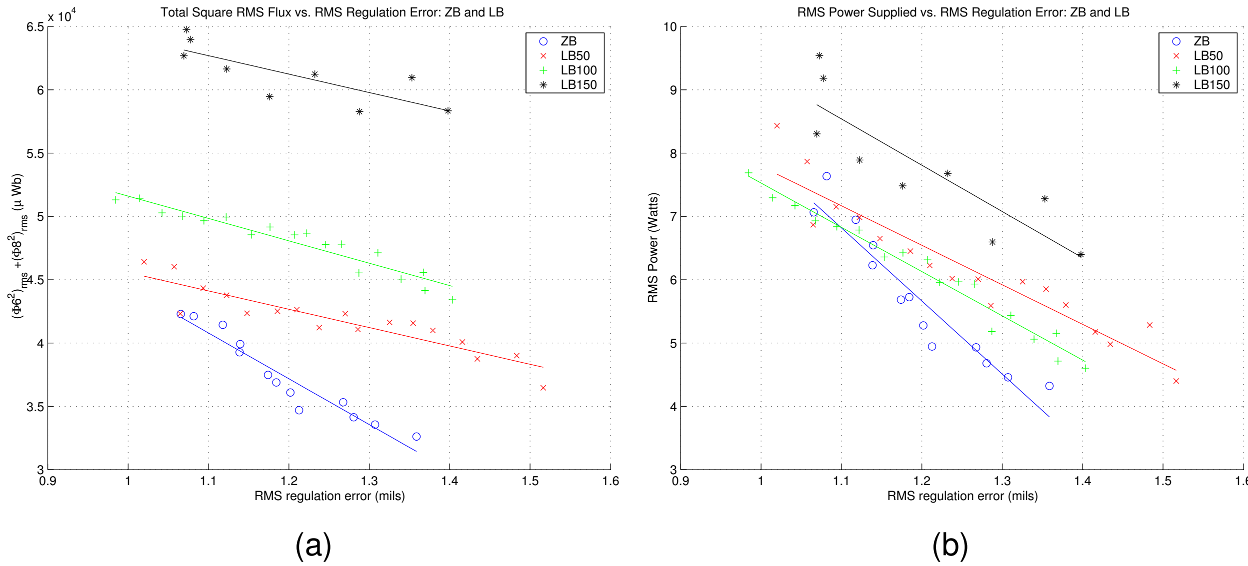

Figure 11. Electrical performance measures vs. regulation performance measure e_{rms} for various Φ_0: (a) total square rms flux $(\Phi_1^2)_{\mathrm{rms}} + (\Phi_2^2)_{\mathrm{rms}}$ vs. e_{rms} (b) rms power consumption $P_{\mathrm{supp,rms}} = (V_{\mathrm{app},1} i_1)_{\mathrm{rms}} + (V_{\mathrm{app},2} i_2)_{\mathrm{rms}}$ vs. e_{rms}

the control flux ϕ.

The experimental data suggests that the rms power consumption behaves according to the sketch in Figure 12. Figure 12a illustrates that for a given rms regulation performance e_{rms}, the power required to implement the control flux, denoted P_ϕ, decreases with increasing Φ_0. This reflects the change in the bearing stiffness with bias flux. Furthermore, for a given Φ_0, the rms control flux power increases when regulating to a tighter error tolerance. In addition, more power is required to implement the bias flux, denoted P_{b}, as the bias increases. The total rms power supplied is $P_{\mathrm{supp,rms}} = P_{\mathrm{b,rms}} + P_{\phi,\mathrm{rms}}$ and is sketched in Figure 12b. This suggests that for a given regulation performance e_{rms}, there exists an optimal bias $\Phi_0^*(e_{\mathrm{rms}})$ that will minimize the AMB rms power consumption.

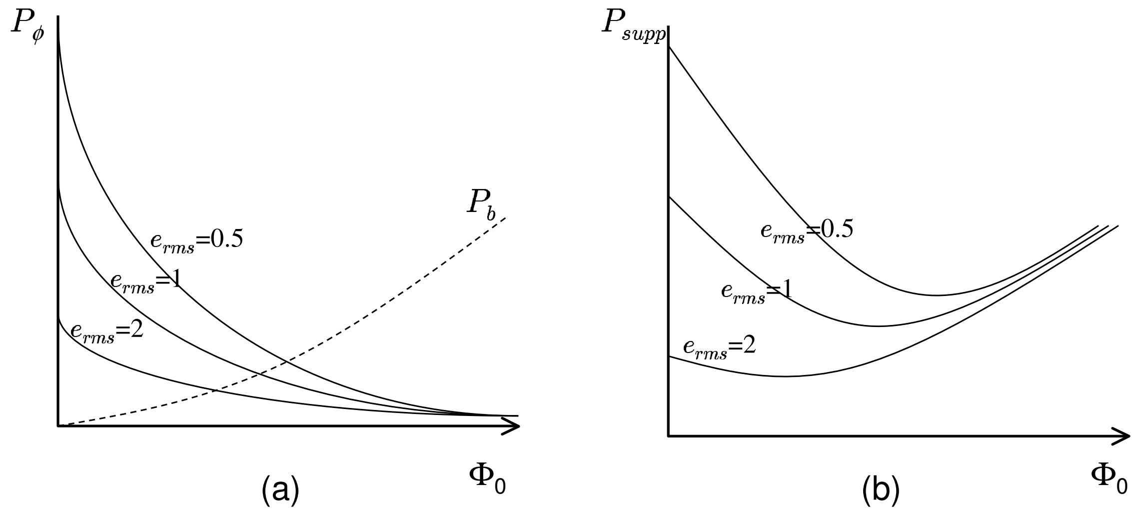

Figure 12. (a) Postulated dependence of the rms power components P_b and P_ϕ on the bias Φ_0. (b) Postulated dependence of the rms power supplied P_{supp} on Φ_0.

VI. Conclusion and Future Work

Control design for the AMB is a two step process: first, a constraint must be designed (which typically implements a bias flux) so that the generation of the net electromagnet force is well-defined. Next, a stabilizing control law is constructed. Since the power loss mechanisms for the FWB and AMB are proportional to the bias flux employed in step 1, it is imperative to reduce the bias flux to realize an FWB with efficient energy storage. Since the standard CFS constraint is a poor choice for low-loss AMB design, the GCFC is used. With the GCFC, one may operate the AMB with a large bias (to obtain some desired bearing stiffness and force slew-rate) or with a small bias (to achieve efficient AMB and FWB operation). In fact, using the GCFC, one may operate with zero bias-flux and still maintain controllability.

The challenges posed to the control design by the low bearing stiffness in ZB and LB must also be addressed. Specifically, when using voltage-mode amplifiers in ZB operation, one must preclude the existence singularities in the control law which induce infinite voltage commands whenever the state trajectory intersects the singularity space. It was experimentally shown that the backstepping control law of equation (31), which is singular on a plane in $\mathbb{R}^3$ in ZB operation ($\overline{\mathcal{D}}_2$), produces unreasonably large control voltage "spikes" that often lead to instability. On the other hand, the CLF control law's singularity space is much smaller than that of the backstepping control law: $\overline{\mathcal{D}}_3$ is a line in $\mathbb{R}^3$. Consequently, the CLF control law rarely generates voltage "spikes" and has much better regulation performance in ZB. Furthermore, the passivity-based control law is completely nonsingular on $\mathbb{R}^3$ and generates finite voltage commands. Finally, the frequency content of the control laws in ZB is used as another way to characterize the singularity behavior. It is found that control laws with smaller singularity spaces require less bandwidth from a voltage-mode amplifier to implement.

When using the GCFC, it is important to understand the effect of the bias value on the AMB mechanical performance measures (bearing stiffness, damping, force slew-rate) and electrical performance measures (energy consumption and efficiency) so that one may evaluate the meaning of each measure according to the requirements of the AMB application. Experiments using the passivity based control law indicate that bearing stiffness indeed increases with bias. When considering the rms power consumption $P_{\mathrm{supp,rms}}$ in terms of its components $P_{\mathrm{b,rms}}$ and $P_{\phi,\mathrm{rms}}$, the rms power required to implement the bias flux $P_{\mathrm{b,rms}}$ increases with increasing Φ_0; on the other hand, the rms power required to implement the control flux $P_{\phi,\mathrm{rms}}$ decreases with increasing Φ_0 because of the corresponding increase in bearing stiffness. As a result, there exists an optimal value $\Phi_0^*(e_{\mathrm{rms}})$, which depends on the regulation performance measure e_{rms}, that minimizes the rms power consumption $P_{\mathrm{supp,rms}}$. Future work includes the determination of this optimal bias flux value.

References

[1] Dassaux, M., "The Industrial Applications of the Active Magnetic Bearings Technology," *Proceedings of the 2nd International Symposium on Magnetic Bearings*, July 1990, pp. 33–38, Tokyo, Japan.

[2] Knospe, C. R. and Fittro, R. L., "Control of a High Speed Milling Spindle via Mu-Synthesis," *Proc. of the 1997 IEEE Intl. Conf. on Contr. Apps.*, 1997, pp. 912–917, Hartford, CT.

[3] Darling, J. and Burrows, C. R., "The Control of Propeller-Induced Vibrations in Ship Transmission Shafts," *Proceedings of the 2nd International Symposium on Magnetic Bearings*, July 1990, pp. 169–174, Tokyo, Japan.

[4] Higuchi, T., Horikoshi, A., and Komori, T., "Development of an Actuator for Super Clean Rooms and Ultra High Vacua," *Proceedings of the 2nd International Symposium on Magnetic Bearings*, July 1990, pp. 115–122, Tokyo, Japan.

[5] Herbner, R., Beno, J., and Walls, A., "Flywheel Batteries Come Around Again," *IEEE Spectrum*, April 2002, pp. 46–51.

[6] Fausz, J., "Control Issues in Simultaneous Attitude Control and Energy Storage," Air Force Research Labs Summer Seminar Series on Structures and Control.

[7] McLallin, K. L., Soeder, J. F., and Jansen, R., "NASA Aerospace Flywheel IPACS Program," Tech. rep., NASA Glenn Research Center, 2000.

[8] Wilson, B. C., Babuška, V., Potter, C., and Fausz, J. L., "Power System Design for a Spacecraft Simulator using Energy Storage Flywheels," *3rd International Energy Conversion Engineering Conference*, AIAA, Aug. 2005, San Francisco, CA.

[9] Fausz, J. L., deBlonk, B. J., Babuška, V., and Fuentes, R. J., "FACETS Demonstration on AMPSS Facility, System Description Document- Release 1.4," Tech. rep., Air Force Research Laboratory, Space Vehicles Directorate, Spacecraft Component Technologies (VSSV), May 2005.

[10] Li, L., "Linearizing Magnetic Bearing Actuators by Constant Current Sum, Constant Voltage Sum, and Constant Flux Sum," *IEEE Trans. Magn.*, Vol. 35, No. 1, Jan. 1999, pp. 528–535.

[11] Tsiotras, P. and Wilson, B. C., "Zero- and Low-Bias Control Designs for Active Magnetic Bearings," *IEEE Trans. Contr. Syst. Technol.*, Vol. 11, No. 6, Nov. 2003, pp. 889–904.

[12] Wilson, B. C. D., Tsiotras, P., and Ferri-Heck, B. S., "Implementation of the Generalized Complementary Flux Constraint for Low-Loss Active Magenetic Bearings," *Proc. of the AIAA Guidance, Navigation,and Control Conf.*, aug 2005, to be published.

[13] Wilson, B. C. D., *Control Designs for Low-Loss Active Magnetic Bearings: Theory and Implementation*, Ph.D. thesis, Georgia Institute of Technology, May 2004.

[14] Charara, A., De Miras, J., and Caron, B., "Nonlinear Control of a Magnetic Levitation System Without Premagetization," *IEEE Trans. Contr. Syst. Technol.*, Vol. 4, No. 5, Sept. 1996, pp. 513–523.

[15] de Queiroz, M. S. and Dawson, D. M., "Nonlinear Control of Active Magnetic Bearings: A Backstepping Approach," *IEEE Trans. Contr. Syst. Technol.*, Vol. 4, No. 5, Sept. 1996, pp. 545–552.

[16] Lévine, J., Lottin, J., and Ponstart, J. C., "A Nonlinear Approach to the Control of Magnetic Bearings," *IEEE Trans. Contr. Syst. Technol.*, Vol. 4, No. 5, Sept. 1996, pp. 524–544.

[17] Wouterse, J. H., "Critical Torque and Speed of Eddy Current Brake with Widely Separated Soft Iron Poles," *IEE Proceedings B (Electric Power Applications)*, Vol. 138, July 1991, pp. 153–158.

[18] Brown, D. and Hamilton III, E. P., *Electromechanical Energy Conversion*, MacMillian Publishing Company, New York, NY, 1984.

[19] Fitzgerald, A. E., Kingsley Jr., C., and Umans, S. D., *Electric Machinery*, McGraw-Hill, Inc., New York, NY, 5th ed., 1990.

[20] Knospe, C., "The Nonlinear Control Benchmark Experiment," *Proceedings of the American Control Conference*, 2000, pp. 2134–2138, Chicago, IL.

[21] Maslen, E., Herman, P., Scott, M., and Humphris, R., "Practical Limits to the Performance of Magnetic Bearings: Peak Force, Slew Rate, and Displacement Sensitivity," *Transactions of the ASME Journal of Tribology*, Vol. 111, 1989, pp. 331–336.

[22] Bornstein, K., "Dynamic Load Capabilities of Active Electromagnetic Bearings," *Transactions of the ASME Journal of Tribology*, Vol. 113, 1991, pp. 598–603.

[23] Vance, J. M., *Rotordynamics of Turbomachinery*, John Wiley and Sons, Inc., 1988, A Wiley-Interscience Publication.

[24] Praly, L., d'Andréa-Novel, B., and Coron, J. M., "Lyapunov Design of Stabilizing Controllers for Cascaded Systems," *IEEE Trans. Automat. Contr.*, Vol. 36, No. 10, 1991, pp. 1177–1181.